

# Spin Delocalisation and the Geometry of Redox-active Cyanomanganese carbonyl Ligands in Heteropolynuclear Complexes of Rhodium(I) \*

Francis L. Atkinson, Aristides Christofides, Neil G. Connelly, Holly J. Lawson,  
Andrew C. Loynes, A. Guy Orpen, Georgina M. Rosair and Gillian H. Worth  
School of Chemistry, University of Bristol, Bristol BS8 1TS, UK

The reactions of *trans*-[Mn(CN)(CO)(dppm)<sub>2</sub>] (dppm = Ph<sub>2</sub>PCH<sub>2</sub>PPh<sub>2</sub>) and *cis*- or *trans*-[Mn(CN)(CO)<sub>2</sub>(PR<sub>3</sub>)(L-L)] [R = OEt or OPh, L-L = dppm; R = Et, L-L = dppe (Ph<sub>2</sub>PCH<sub>2</sub>CH<sub>2</sub>PPh<sub>2</sub>)] with [{Rh(μ-Cl)(CO)<sub>2</sub>}<sub>2</sub>] give the heterobinuclear complexes [*trans*-(dppm)<sub>2</sub>(OC)Mn(μ-CN)Rh(CO)<sub>2</sub>Cl] and [(L-L)(R<sub>3</sub>P)(OC)<sub>2</sub>Mn(μ-CN)Rh(CO)<sub>2</sub>Cl] respectively. Cyclic voltammetry shows that each complex undergoes oxidation at the manganese centre; chemical oxidation of [*trans*-(dppm)<sub>2</sub>(OC)Mn(μ-CN)Rh(CO)<sub>2</sub>Cl] gives [*trans*-(dppm)<sub>2</sub>(OC)Mn(μ-CN)Rh(CO)<sub>2</sub>Cl]<sup>+</sup> which may also be prepared from *trans*-[Mn(CN)(CO)(dppm)<sub>2</sub>]<sup>+</sup> and [{Rh(μ-Cl)(CO)<sub>2</sub>}<sub>2</sub>]. The crystal structures of the redox pair [*trans*-(dppm)<sub>2</sub>(OC)Mn(μ-CN)Rh(CO)<sub>2</sub>Cl]<sup>z</sup> (Z = 0 or +1) show that substantial changes in geometry resulting from oxidation are limited to the vicinity of the manganese atoms (e.g. mean Mn-P increases from 2.284 to 2.352 Å). These changes are similar to those observed for the free cyanomanganese complexes *trans*-[Mn(CN)(CO)(dppm)<sub>2</sub>]<sup>z</sup> (Z = 0 or +1) and indicate that the singly occupied molecular orbital in the radical cation is largely composed of the Mn d<sub>z</sub> orbital in the MnP<sub>4</sub> plane. Changes in geometry in the Mn(μ-CN)Rh(CO)<sub>2</sub>Cl unit are very small. Treatment of [*cis*-(L-L)(R<sub>3</sub>P)(OC)<sub>2</sub>Mn(μ-CN)Rh(CO)<sub>2</sub>Cl] or [*trans*-(L-L)(R<sub>3</sub>P)(OC)<sub>2</sub>Mn(μ-CN)Rh(CO)<sub>2</sub>Cl] with TiPF<sub>6</sub> in the presence of [Mn(CN)(CO)<sub>2</sub>(PR<sub>3</sub>)(L-L)] gives the heterotrinuclear cations [{(L-L)(R<sub>3</sub>P)(OC)<sub>2</sub>Mn(μ-CN)}<sub>2</sub>Rh(CO)<sub>2</sub>]<sup>+</sup>; the crystal structure of one, [{*trans*-(dppm)[(EtO)<sub>3</sub>P]}(OC)<sub>2</sub>Mn(μ-CN)<sub>2</sub>Rh(CO)<sub>2</sub>], shows the two cyanomanganese ligands *cis*-co-ordinated to the rhodium centre. Cyclic, differential-pulse, and square-wave voltammetry of [{*trans*-(dppm)(R<sub>3</sub>P)(OC)<sub>2</sub>Mn(μ-CN)}<sub>2</sub>Rh(CO)<sub>2</sub>]<sup>+</sup> (R = OEt or OPh) show two closely spaced oxidation waves; the small separation (ca. 80–90 mV) suggests weak interaction between the two cyanomanganese ligands in the mixed-valence dication [{*trans*-(dppm)(R<sub>3</sub>P)(OC)<sub>2</sub>Mn(μ-CN)}<sub>2</sub>Rh(CO)<sub>2</sub>]<sup>2+</sup> (R = OEt or OPh). The results provide evidence for the dependence of spin delocalisation from Mn<sup>II</sup> to Rh<sup>I</sup> on the geometry of the ancillary ligands bound to manganese.

We have recently described the synthesis, electrochemical properties<sup>1</sup> and electronic structure<sup>2</sup> of homobinuclear cyanobridged dimanganese complexes such as 1<sup>+</sup> and shown how studies of the oxidatively induced *cis*-*trans* isomerisation of the individual manganese centres provide insight into the extent of intermetallic interaction in the mixed-valence dications 1<sup>2+</sup>. We have also shown<sup>3</sup> that intramolecular electron transfer via the cyanide bridge occurs between metal (Mn) and ligand (catecholatoruthenium) redox sites in heterobinuclear complexes such as 2. We now discuss a third type of complex where the cyanomanganese ligands are bound to redox-inert, square-planar rhodium(I). Thus, we give details<sup>4</sup> of the syntheses of the heterobinuclear complexes [*trans*-(dppm)<sub>2</sub>(OC)Mn(μ-CN)-Rh(CO)<sub>2</sub>Cl]<sup>z</sup> (Z = 0, 3 or +1, 3<sup>+</sup>; dppm = Ph<sub>2</sub>PCH<sub>2</sub>PPh<sub>2</sub>), [*trans*-(dppm){(RO)<sub>3</sub>P}(OC)<sub>2</sub>Mn(μ-CN)Rh(CO)<sub>2</sub>Cl]<sup>+</sup> 4 (R = Et or Ph), [*cis*-(dppm){(RO)<sub>3</sub>P}(OC)<sub>2</sub>Mn(μ-CN)Rh(CO)<sub>2</sub>Cl]<sup>5</sup> (R = Et or Ph) and the heterotrinuclear cations [{(L-L)-(R<sub>3</sub>P)(OC)<sub>2</sub>Mn(μ-CN)}<sub>2</sub>Rh(CO)<sub>2</sub>]<sup>+</sup> (L-L = dppm, R = OEt

or OPh; L-L = Ph<sub>2</sub>PCH<sub>2</sub>CH<sub>2</sub>PPh<sub>2</sub> = dppe, R = Et), the X-ray structures of the redox pair 3 and 3<sup>+</sup> and of [{*trans*-(dppm)[(EtO)<sub>3</sub>P]}(OC)<sub>2</sub>Mn(μ-CN)<sub>2</sub>Rh(CO)<sub>2</sub>]<sup>+</sup>, and electrochemical and spectroscopic studies which reveal (i) little interaction between Mn and Rh in the bimetallic species 3<sup>+</sup> but (ii) weak interaction, via the Rh(CO)<sub>2</sub> bridge, between the two manganese centres in [{*trans*-(dppm)(R<sub>3</sub>P)(OC)<sub>2</sub>Mn(μ-CN)}<sub>2</sub>Rh(CO)<sub>2</sub>]<sup>2+</sup> (R = OEt or OPh). The results provide evidence for the dependence of spin localisation from manganese(II) to rhodium(I) on the geometry of the ancillary ligands bound to manganese.

## Results and Discussion

**Heterobinuclear Complexes.**—The addition of *trans*-[Mn(CN)(CO)(dppm)<sub>2</sub>], *trans*- or *cis*-[Mn(CN)(CO)<sub>2</sub>(PR<sub>3</sub>)(dppm)] (R = OEt or OPh) or *cis*-[Mn(CN)(CO)<sub>2</sub>(PEt<sub>3</sub>)(dppe)] to [{Rh(μ-Cl)(CO)<sub>2</sub>}<sub>2</sub>] in CH<sub>2</sub>Cl<sub>2</sub> immediately gave yellow solutions from which good yields of the heterobinuclear complexes [*trans*-(dppm)<sub>2</sub>(OC)Mn(μ-CN)Rh(CO)<sub>2</sub>Cl] 3, [*trans*-(dppm){(RO)<sub>3</sub>P}(OC)<sub>2</sub>Mn(μ-CN)Rh(CO)<sub>2</sub>Cl]<sup>+</sup> 4 (R = Et or Ph), [*cis*-(dppm){(RO)<sub>3</sub>P}(OC)<sub>2</sub>Mn(μ-CN)Rh(CO)<sub>2</sub>Cl]<sup>5</sup> (R = Et or Ph) and [*cis*-(dppe)(Et<sub>3</sub>P)(OC)<sub>2</sub>Mn(μ-CN)Rh(CO)<sub>2</sub>Cl] were isolated as air-stable, yellow solids (Table 1). In each case the geometries of the individual metal carbonyl units were readily deduced from their IR carbonyl spectra; the two bands associated with the *cis*-Rh(CO)<sub>2</sub> group are essentially

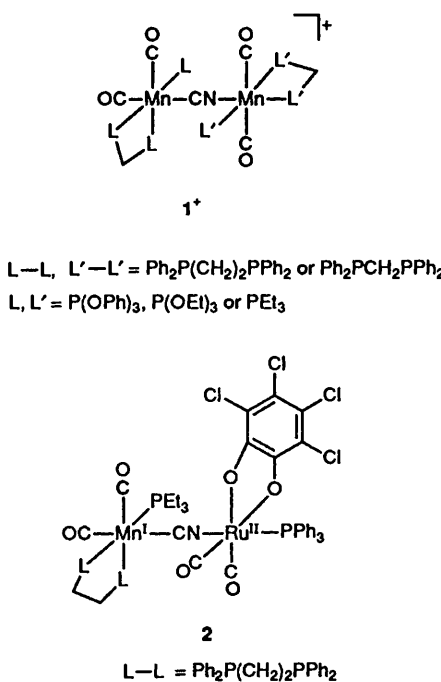
\* Supplementary data available: see Instructions for Authors, *J. Chem. Soc., Dalton Trans.*, 1993, Issue 1, pp. xxiii–xxviii.

In the heterobi- and tri-nuclear complexes described herein the prefixes *cis* and *trans* refer to the geometry of the manganese dicarbonyl group. {The cyanide and carbonyl ligands are *trans*-disposed in *trans*-[Mn(CN)(CO)(dppm)<sub>2</sub>].} In all cases the Rh(CO)<sub>2</sub> group has *cis*-carbonyl ligands.

**Table 1** Analytical and IR spectroscopic data for  $[\{L_xMn(\mu-CN)\}_nRh(CO)_2Cl_{2-n}]^z$ 

$L_x$	$n$	$Z^a$	Colour	Yield (%)	Analysis (%) <sup>b</sup>			IR $\text{cm}^{-1}$		
					C	H	N	$\nu(CN)^d$	$\nu(CO)(Rh)$	$\nu(CO)(Mn)$
<i>cis</i> -(CO) <sub>2</sub> {P(OPh) <sub>3</sub> }(dppm) <b>5</b> (R = Ph)	1	0	Yellow	62	55.0 (55.0)	3.6 (3.6)	1.4 (1.4)	2128	2079, 2008	1975, 1923
<i>cis</i> -(CO) <sub>2</sub> {P(OEt) <sub>3</sub> }(dppm) <b>5</b> (R = Et)	1	0	Yellow	65	48.6 (49.0)	4.2 (4.2)	1.5 (1.6)	2123	2080, 2007	1963, 1908
<i>cis</i> -(CO) <sub>2</sub> (PEt <sub>3</sub> )(dppe)	1	0	Yellow	60	52.2 (52.4)	5.0 (4.6)	1.6 (1.7)	2118	2079, 2008	1944, 1887
<i>trans</i> -(CO) <sub>2</sub> {P(OPh) <sub>3</sub> }(dppm) <b>4</b> (R = Ph)	1	0	Yellow	67	56.2 (56.2)	3.6 (3.6)	1.4 (1.4)	2118	2079, 2008	1940
<i>trans</i> -(CO) <sub>2</sub> {P(OEt) <sub>3</sub> }(dppm) <b>4</b> (R = Et)	1	0	Yellow	71	49.1 (49.0)	4.6 (4.2)	1.5 (1.6)	2106	2078, 2006	1925
<i>trans</i> -(CO)(dppm) <sub>2</sub> <b>3</b> <sup>e</sup>	1	0	Beige	47	58.7 (58.2)	4.1 (4.4)	1.3 (1.2)	2102	2076, 2004	1874 (m)
<i>trans</i> -(CO)(dppm) <sub>2</sub> <b>3</b> <sup>+</sup>	1	1	Red	70	53.1 (53.3)	3.7 (3.6)	1.2 (1.2)	2136	2085, 2014	1948 (m)
<i>cis</i> -(CO) <sub>2</sub> {P(OPh) <sub>3</sub> }(dppm) <b>8</b>	2	1	Yellow	72	57.4 (57.4)	4.0 (3.8)	1.4 (1.4)	2110	2091, 2025	1977, 1925
<i>cis</i> -(CO) <sub>2</sub> (PEt <sub>3</sub> )(dppe)	2	1	Yellow	71	52.9 (53.7)	4.8 (4.8)	1.8 (1.7)	2106	2087, 2002	1948, 1892
<i>trans</i> -(CO) <sub>2</sub> {P(OPh) <sub>3</sub> }(dppm) <b>7</b> (R = Ph)	2	1	Orange	85	57.2 (57.4)	4.0 (3.8)	1.6 (1.4)	<i>f</i>	2087, 2024	1941
<i>trans</i> -(CO) <sub>2</sub> {P(OEt) <sub>3</sub> }(dppm) <b>7</b> (R = Et)	2	1	Yellow	85	50.4 (50.1)	4.3 (4.4)	1.7 (1.7)	<i>f</i>	2086, 2023	1927

<sup>a</sup> Cationic complexes analysed as  $[PF_6]^-$  salts. <sup>b</sup> Calculated values in parentheses. <sup>c</sup> In  $\text{CH}_2\text{Cl}_2$ . Strong absorptions unless stated otherwise; m = medium. <sup>d</sup> Weak. <sup>e</sup> Sample analysed as a 0.5  $\text{CH}_2\text{Cl}_2$  solvate. <sup>f</sup> Ill defined shoulder on the high energy carbonyl absorption of the  $Rh(CO)_2$  group.



independent of the nature of the ligands on the manganese centre whereas those of the  $Mn(\text{CO})_2$  moiety vary with both the geometry of the complex (two bands for the *cis* isomers, one for *trans* isomers) and the nature of the bonded P donors. As observed<sup>3</sup> previously, the cyanide absorption increases in intensity and shifts to higher energy on bridge formation; the shift in energy is also dependent on the ancillary ligands on manganese.

The cyclic voltammetry of  $[\text{trans-}(dppm)\{(\text{RO})_3\text{P}\}(\text{OC})_2\text{Mn}(\mu-\text{CN})\text{Rh}(\text{CO})_2\text{Cl}]$  is straightforward; the  $\text{P}(\text{OEt})_3$  complex shows a reversible oxidation wave [ $(i_p)_{\text{red}}/(i_p)_{\text{ox}} = 1.0$  for scan rates,  $v$ , from 50 to 200  $\text{mV s}^{-1}$ ] centred at 0.74 V whereas the corresponding wave for the  $\text{P}(\text{OPh})_3$  analogue, centred at 0.92 V, is incompletely chemically reversible [ $(i_p)_{\text{red}}/(i_p)_{\text{ox}} = 0.79$ ,  $v = 50 \text{ mV s}^{-1}$ ;  $(i_p)_{\text{red}}/(i_p)_{\text{ox}} = 0.93$ ,  $v = 200 \text{ mV s}^{-1}$ ] suggesting that  $[\text{trans-}(dppm)\{(\text{PhO})_3\text{P}\}(\text{OC})_2\text{Mn}(\mu-\text{CN})\text{Rh}(\text{CO})_2\text{Cl}]^+$  is less stable than  $[\text{trans-}(dppm)\{(\text{EtO})_3\text{P}\}(\text{OC})_2\text{Mn}(\mu-\text{CN})\text{Rh}(\text{CO})_2\text{Cl}]^+$ . For both neutral complexes, the oxidation potential is considerably more positive than that of the corresponding free manganese ligands (*i.e.*  $\text{trans-}[\text{Mn}(\text{CN})(\text{CO})_2\{\text{P}(\text{OEt})_3\}(\text{dppm})]$ ,  $E^\circ = 0.50$  V;  $\text{trans-}[\text{Mn}(\text{CN})(\text{CO})_2\{\text{P}(\text{OPh})_3\}(\text{dppm})]$ ,  $E^\circ = 0.64$  V) as previously

observed when the cyanide nitrogen atom is metal-coordinated.<sup>4</sup>

The cyclic voltammograms of  $[\text{cis-}(dppm)\{(\text{RO})_3\text{P}\}(\text{OC})_2\text{Mn}(\mu-\text{CN})\text{Rh}(\text{CO})_2\text{Cl}]$  ( $R = \text{Et}$  or  $\text{Ph}$ ) and  $[\text{cis-}(dppe)\{(\text{Et})_3\text{P}\}(\text{OC})_2\text{Mn}(\mu-\text{CN})\text{Rh}(\text{CO})_2\text{Cl}]$  are qualitatively similar to those of the corresponding mononuclear cyanomanganese ligands in that irreversible oxidation waves are accompanied by product waves at more negative potentials, consistent with *cis-trans* oxidative isomerisation at manganese. However, the voltammetric behaviour of the heterobinuclear species differs in that additional waves are also observed. Thus, for example,  $[\text{cis-}(dppm)\{(\text{EtO})_3\text{P}\}(\text{OC})_2\text{Mn}(\mu-\text{CN})\text{Rh}(\text{CO})_2\text{Cl}]$  shows two oxidation waves, with peak potentials of 1.17 and 1.24 V (at a scan rate of 200  $\text{mV s}^{-1}$ ), accompanied by a broad product peak at 0.71 V. On the second and subsequent scans new oxidation peaks are observed at 0.78 and 0.85 V. The product peaks at 0.78 (oxidation) and 0.71 V (reduction) correspond to those for the couple  $[\text{trans-}(dppm)\{(\text{EtO})_3\text{P}\}(\text{OC})_2\text{Mn}(\mu-\text{CN})\text{Rh}(\text{CO})_2\text{Cl}]^- - [\text{trans-}(dppm)\{(\text{EtO})_3\text{P}\}(\text{OC})_2\text{Mn}(\mu-\text{CN})\text{Rh}(\text{CO})_2\text{Cl}]^+$ ; the cation is the expected product from the oxidative isomerisation of  $[\text{cis-}(dppm)\{(\text{EtO})_3\text{P}\}(\text{OC})_2\text{Mn}(\mu-\text{CN})\text{Rh}(\text{CO})_2\text{Cl}]$ . The source of the other additional waves is unknown though the use of analytically pure, crystalline samples of  $[\text{cis-}(dppm)\{(\text{RO})_3\text{P}\}(\text{OC})_2\text{Mn}(\mu-\text{CN})\text{Rh}(\text{CO})_2\text{Cl}]$  in the electrochemical studies suggest that they are due to product formation after oxidation rather than to reaction before electron transfer or to the presence of impurities. The additional waves are at more positive potentials than those of the free cyanomanganese ligands implying that the cyanide nitrogen atom is still coordinated in the unknown product. Moreover, the relative stability of the manganese(II)-containing cations  $[\text{trans-}(dppm)\{(\text{RO})_3\text{P}\}(\text{OC})_2\text{Mn}(\mu-\text{CN})\text{Rh}(\text{CO})_2\text{Cl}]^+$  (see above) suggests that, on oxidation, reaction occurs at the cyanide nitrogen atom of  $[\text{cis-}(dppm)\{(\text{PhO})_3\text{P}\}(\text{OC})_2\text{Mn}(\mu-\text{CN})\text{Rh}(\text{CO})_2\text{Cl}]^+$  before isomerisation. There is, therefore, the additional implication that the  $Mn^{II}(\mu-\text{CN})\text{Rh}$  linkage is more robust with a *trans*-(dppm)( $\text{R}_3\text{P}$ )( $\text{OC}$ )<sub>2</sub> ligand set rather than a *cis*-(dppm)( $\text{R}_3\text{P}$ )( $\text{OC}$ )<sub>2</sub> ligand set, at least on the cyclic voltammetric time-scale. More detailed, quantitative, electrochemical studies will be required to unravel this complex behaviour.

By contrast to the results described above, the oxidation of  $[\text{trans-}(dppm)_2(\text{OC})\text{Mn}(\mu-\text{CN})\text{Rh}(\text{CO})_2\text{Cl}]$  **3** is well defined. The cyclic voltammogram shows one fully reversible one-electron oxidation wave and the potential for the process ( $E^\circ = 0.21$  V) is such that the monocation is readily generated from  $[\text{trans-}(dppm)_2(\text{OC})\text{Mn}(\mu-\text{CN})\text{Rh}(\text{CO})_2\text{Cl}]$  using the mild oxidant  $[\text{Fe}(\text{n-C}_5\text{H}_5)_2]^+$  in  $\text{CH}_2\text{Cl}_2$ . However, the red, air-stable, paramagnetic (one unpaired electron,  $\mu_{\text{eff}} = 1.97$ ) salt  $[\text{trans-}(dppm)_2(\text{OC})\text{Mn}(\mu-\text{CN})\text{Rh}(\text{CO})_2\text{Cl}][\text{PF}_6]$  (Table 1) is better prepared by reacting  $\text{trans-}[\text{Mn}(\text{CN})(\text{CO})(\text{dppm})_2][\text{PF}_6]$  with  $[\{\text{Rh}(\mu-\text{Cl})(\text{CO})_2\}_2]$ . On oxidising **3** to **3**<sup>+</sup> both the

**Table 2** Selected bond lengths ( $\text{\AA}$ ) and angles ( $^\circ$ ) for [*trans*-(dppm)<sub>2</sub>(OC)Mn( $\mu$ -CN)Rh(CO)<sub>2</sub>Cl]<sup>+</sup> 3

Rh–Cl(1)	2.354(1)	Rh–N(1)	2.043(4)	Rh–C(53)	1.822(5)
Rh–C(54)	1.838(6)	Mn–P(1)	2.283(1)	Mn–P(2)	2.292(1)
Mn–P(3)	2.282(1)	Mn–P(4)	2.276(1)	Mn–C(1)	1.976(4)
Mn–C(2)	1.776(4)	P(1)–C(3)	1.832(5)	P(1)–C(9)	1.828(4)
P(1)–C(15)	1.852(4)	P(2)–C(15)	1.846(5)	P(2)–C(16)	1.831(5)
P(2)–C(22)	1.831(5)	P(3)–C(28)	1.826(5)	P(3)–C(34)	1.842(5)
P(3)–C(40)	1.848(4)	P(4)–C(40)	1.851(5)	P(4)–C(41)	1.827(4)
P(4)–C(47)	1.826(5)	N(1)–C(1)	1.154(5)	O(1)–C(2)	1.175(5)
O(2)–C(53)	1.148(7)	O(3)–C(54)	1.136(8)		
Cl(1)–Rh–N(1)	91.1(1)	Cl(1)–Rh–C(53)	177.5(2)	N(1)–Rh–C(53)	91.3(2)
Cl(1)–Rh–C(54)	87.6(2)	N(1)–Rh–C(54)	178.7(2)	C(53)–Rh–C(54)	89.9(3)
P(1)–Mn–P(2)	72.6(1)	P(1)–Mn–P(3)	177.1(1)	P(2)–Mn–P(3)	107.1(1)
P(1)–Mn–P(4)	107.3(1)	P(2)–Mn–P(4)	178.3(1)	P(3)–Mn–P(4)	72.9(1)
P(1)–Mn–C(1)	86.6(1)	P(2)–Mn–C(1)	85.0(1)	P(3)–Mn–C(1)	90.5(1)
P(4)–Mn–C(1)	93.4(1)	P(1)–Mn–C(2)	91.8(1)	P(2)–Mn–C(2)	94.7(1)
P(3)–Mn–C(2)	91.2(1)	P(4)–Mn–C(2)	87.0(1)	C(1)–Mn–C(2)	178.3(2)
Mn–P(1)–C(3)	128.8(1)	Mn–P(1)–C(9)	116.8(1)	C(3)–P(1)–C(9)	102.6(2)
Mn–P(1)–C(15)	93.2(1)	C(3)–P(1)–C(15)	106.1(2)	C(9)–P(1)–C(15)	106.5(2)
Mn–P(2)–C(15)	93.1(1)	Mn–P(2)–C(16)	122.6(1)	C(15)–P(2)–C(16)	108.1(2)
Mn–P(2)–C(22)	124.2(1)	C(15)–P(2)–C(22)	104.0(2)	C(16)–P(2)–C(22)	102.0(2)
Mn–P(3)–C(28)	118.5(1)	Mn–P(3)–C(34)	128.1(2)	C(28)–P(3)–C(34)	101.3(2)
Mn–P(3)–C(40)	93.5(1)	C(28)–P(3)–C(40)	107.6(2)	C(34)–P(3)–C(40)	105.3(2)
Mn–P(4)–C(40)	93.6(1)	Mn–P(4)–C(41)	124.5(1)	C(40)–P(4)–C(41)	103.9(2)
Mn–P(4)–C(47)	122.7(1)	C(40)–P(4)–C(47)	108.2(2)	C(41)–P(4)–C(47)	101.2(2)
Rh–N(1)–C(1)	176.9(4)	Mn–C(1)–N(1)	178.5(4)	Mn–C(2)–O(1)	178.6(5)
P(1)–C(15)–P(2)	94.2(2)	P(3)–C(40)–P(4)	94.1(2)	Rh–C(53)–O(2)	177.5(5)
Rh–C(54)–O(3)	178.7(6)				

**Table 3** Selected bond lengths ( $\text{\AA}$ ) and angles ( $^\circ$ ) for [*trans*-(dppm)<sub>2</sub>(OC)Mn( $\mu$ -CN)Rh(CO)<sub>2</sub>Cl]<sup>+</sup>[PF<sub>6</sub>]<sup>-</sup>·1.5C<sub>6</sub>H<sub>14</sub> 3<sup>+</sup>PF<sub>6</sub>·1.5C<sub>6</sub>H<sub>14</sub>

Rh–Cl(1)	2.340(2)	Rh–N(1)	2.038(5)	Rh–C(53)	1.817(8)
Rh–C(54)	1.836(8)	Mn–P(1)	2.351(2)	Mn–P(3)	2.341(2)
Mn–P(2)	2.361(2)	Mn–P(4)	2.354(2)	Mn–C(1)	1.964(6)
Mn–C(2)	1.805(6)	P(1)–C(3)	1.809(6)	P(1)–C(9)	1.812(6)
P(1)–C(15)	1.828(6)	P(3)–C(28)	1.814(7)	P(3)–C(34)	1.802(6)
P(3)–C(40)	1.829(6)	P(2)–C(15)	1.834(6)	P(2)–C(16)	1.804(6)
P(2)–C(22)	1.808(6)	P(4)–C(40)	1.835(6)	P(4)–C(41)	1.818(6)
P(4)–C(47)	1.792(6)	O(1)–C(2)	1.140(7)	O(2)–C(53)	1.153(10)
O(3)–C(54)	1.120(10)	N(1)–C(1)	1.148(7)		
Cl(1)–Rh–N(1)	89.4(1)	Cl(1)–Rh–C(53)	176.9(3)	N(1)–Rh–C(53)	90.5(3)
Cl(1)–Rh–C(54)	88.8(3)	N(1)–Rh–C(54)	177.1(3)	C(53)–Rh–C(54)	91.5(3)
P(1)–Mn–P(3)	103.4(1)	P(1)–Mn–P(2)	72.0(1)	P(3)–Mn–P(2)	174.4(1)
P(1)–Mn–P(4)	174.8(1)	P(3)–Mn–P(4)	72.6(1)	P(2)–Mn–P(4)	111.9(1)
P(1)–Mn–C(1)	86.2(2)	P(3)–Mn–C(1)	89.8(2)	P(2)–Mn–C(1)	86.8(2)
P(4)–Mn–C(1)	90.4(2)	P(1)–Mn–C(2)	95.6(2)	P(3)–Mn–C(2)	91.5(2)
P(2)–Mn–C(2)	92.1(2)	P(4)–Mn–C(2)	87.9(2)	C(1)–Mn–C(2)	177.5(3)
Mn–P(1)–C(3)	124.9(2)	Mn–P(1)–C(9)	120.2(2)	C(3)–P(1)–C(9)	102.1(3)
Mn–P(1)–C(15)	91.8(2)	C(3)–P(1)–C(15)	108.2(3)	C(9)–P(1)–C(15)	107.6(3)
Mn–P(3)–C(28)	119.0(2)	Mn–P(3)–C(34)	122.7(2)	C(28)–P(3)–C(34)	105.0(3)
Mn–P(3)–C(40)	92.3(2)	C(28)–P(3)–C(40)	108.6(3)	C(34)–P(3)–C(40)	107.4(3)
Mn–P(2)–C(15)	91.3(2)	Mn–P(2)–C(16)	121.7(2)	C(15)–P(2)–C(16)	107.1(3)
Mn–P(2)–C(22)	120.6(2)	C(15)–P(2)–C(22)	109.1(3)	C(16)–P(2)–C(22)	104.9(3)
Mn–P(4)–C(40)	91.7(2)	Mn–P(4)–C(41)	123.1(2)	C(40)–P(4)–C(41)	106.5(3)
Mn–P(4)–C(47)	119.5(2)	C(40)–P(4)–C(47)	109.0(3)	C(41)–P(4)–C(47)	104.8(3)
Rh–N(1)–C(1)	175.0(5)	Mn–C(1)–N(1)	178.2(5)	Mn–C(2)–O(1)	178.9(5)
P(1)–C(15)–P(2)	98.2(3)	P(3)–C(40)–P(4)	98.6(3)	Rh–C(53)–O(2)	178.1(7)
Rh–C(54)–O(3)	178.0(8)				

carbonyl band associated with the manganese-bound CO ligand and the bridging cyanide band are shifted to higher energy (by *ca.* 75 and 35 cm<sup>-1</sup> respectively). The carbonyl bands associated with the *cis*-Rh(CO)<sub>2</sub> moiety are also shifted to higher energy but by only *ca.* 10 cm<sup>-1</sup>. The anisotropic ESR spectrum of [*trans*-(dppm)<sub>2</sub>(OC)Mn( $\mu$ -CN)Rh(CO)<sub>2</sub>Cl]<sup>+</sup> is very similar to that of the manganese(II) ligand *trans*-[Mn(CN)(CO)(dppm)<sub>2</sub>]<sup>+</sup> itself.<sup>5</sup> This, taken with the IR spectroscopic data noted above, suggests that manganese-based oxidation results in a small increase in positive charge at rhodium but little delocalisation of unpaired electron density.

The isolation of both members of the redox pair [*trans*-(dppm)<sub>2</sub>(OC)Mn( $\mu$ -CN)Rh(CO)<sub>2</sub>Cl]<sup>+</sup> 3 and [*trans*-(dppm)<sub>2</sub>(OC)Mn( $\mu$ -CN)Rh(CO)<sub>2</sub>Cl]<sup>+</sup> 3<sup>+</sup> (as a hexane solvate of its [PF<sub>6</sub>]<sup>-</sup> salt) in crystalline form provided an opportunity to probe the effects of oxidation more fully. The results of the crystal structure analyses are summarised in Tables 2 and 3 and illustrated in Figs. 1 and 2. In both structures the geometries at the metals are based on the expected octahedral arrangement at manganese and square-planar co-ordination at rhodium. The largest angular distortions involve the small bite angle (*ca.* 72.5°) of the chelating dppm ligands at manganese. The chair-like folding of the pair of four-membered rings in the CP<sub>2</sub>-MnP<sub>2</sub>C systems of [*trans*-(dppm)<sub>2</sub>(OC)Mn( $\mu$ -CN)Rh(CO)<sub>2</sub>Cl]<sup>+</sup> and [*trans*-(dppm)<sub>2</sub>(OC)Mn( $\mu$ -CN)Rh(CO)<sub>2</sub>Cl]<sup>3+</sup> (angles between MnP<sub>2</sub> and P<sub>2</sub>C planes of 27.2 and 25.2° for 3, and 27.0

(OC)Mn( $\mu$ -CN)Rh(CO)<sub>2</sub>Cl]<sup>3+</sup> (as a hexane solvate of its [PF<sub>6</sub>]<sup>-</sup> salt) in crystalline form provided an opportunity to probe the effects of oxidation more fully. The results of the crystal structure analyses are summarised in Tables 2 and 3 and illustrated in Figs. 1 and 2. In both structures the geometries at the metals are based on the expected octahedral arrangement at manganese and square-planar co-ordination at rhodium. The largest angular distortions involve the small bite angle (*ca.* 72.5°) of the chelating dppm ligands at manganese. The chair-like folding of the pair of four-membered rings in the CP<sub>2</sub>-MnP<sub>2</sub>C systems of [*trans*-(dppm)<sub>2</sub>(OC)Mn( $\mu$ -CN)Rh(CO)<sub>2</sub>Cl]<sup>+</sup> and [*trans*-(dppm)<sub>2</sub>(OC)Mn( $\mu$ -CN)Rh(CO)<sub>2</sub>Cl]<sup>3+</sup> (angles between MnP<sub>2</sub> and P<sub>2</sub>C planes of 27.2 and 25.2° for 3, and 27.0

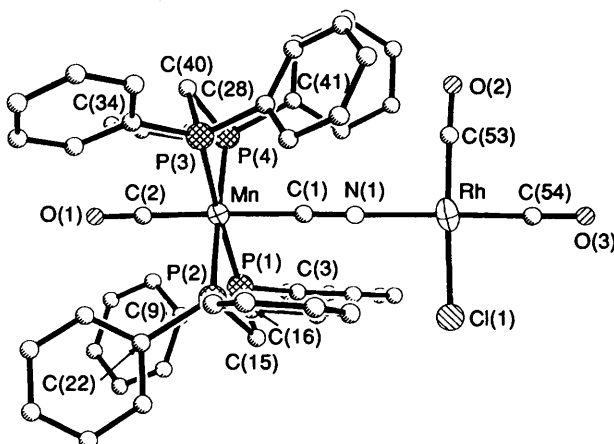


Fig. 1 Molecular structure of 3 showing the atom labelling scheme. All of the hydrogen atoms have been omitted for clarity

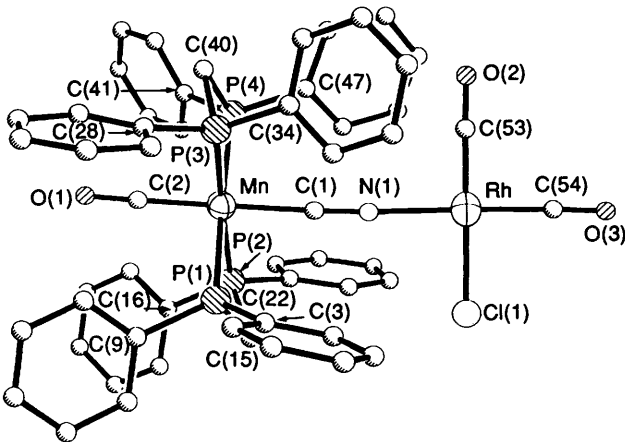


Fig. 2 Molecular structure of 3<sup>+</sup> showing the atom labelling scheme. All of the hydrogen atoms have been omitted for clarity

and 23.2° for 3<sup>+</sup>) is clear {see Figs. 1 and 2 and cf. the structures of [Mn(CN)(CO)(dppm)<sub>2</sub>]<sup>Z</sup> ( $Z = 0$ , 6 or +1 6<sup>+</sup>)}.<sup>5</sup> The co-ordination planes of the rhodium atoms lie approximately perpendicular to the MnP<sub>4</sub> units (dihedral angles 91.9 and 94.5° for 3 and 3<sup>+</sup>) allowing the substituents at rhodium to occupy the crevice between the phenyl rings of the dppm ligands.

There are some aspects of the molecular geometry of 3 which are noticeably perturbed by oxidation. The most striking feature is the large increase in the Mn–P distances (mean for 3 2.284, for 3<sup>+</sup> 2.352 Å) on oxidation, which is accompanied by slight decreases in the average P–C distances (mean P–C<sub>i,pso</sub> 1.830 and P–CH<sub>2</sub> 1.849 Å for 3, cf. 1.807 and 1.852 Å for 3<sup>+</sup>) and increases in the average C–P–C angle (104.7° for 3 to 106.7° for 3<sup>+</sup>). These changes are similar to those we have observed<sup>6</sup> and discussed<sup>7</sup> for other phosphine containing redox pairs and the absolute values are very close to those observed for [Mn(CN)(CO)(dppm)<sub>2</sub>]<sup>Z</sup> ( $Z = 0$ , 6 or +1 6<sup>+</sup>).<sup>5</sup> Thus the mean Mn–P distance for 6 is 2.270 Å (2.346 Å for 6<sup>+</sup>), the average P–C distances for 6 are P–C<sub>i,pso</sub> 1.832 and P–CH<sub>2</sub> 1.852 Å, cf. 1.813 and 1.846 Å for 6<sup>+</sup>, and the average C–P–C angles are 104.3° for 6 and 106.8° for 6<sup>+</sup>. These observations allow use of, for example, the mean Mn–P distance as a structural measure of the oxidation state of the {Mn(CN)(CO)(dppm)<sub>2</sub>} moiety when present as a ligand. The geometry changes noted above are consistent with oxidation causing depopulation of the Mn d<sub>z</sub> orbital in the plane of the dppm ligands, which is involved in Mn–P π-back-bonding.

Other bond length and geometry changes on oxidation are small. Thus the Mn–CO distance increases slightly on oxidation of 3 to 3<sup>+</sup> [from 1.776(4) to 1.805(6) Å, cf. 1.813(15) Å in 6<sup>+</sup>], while the Mn–CN distance decreases by less than 2σ [from

1.976(4) to 1.964(6) Å, cf. 1.964(13) Å in 6<sup>+</sup>]. The C–N and C–O distances are essentially unaffected [the C–O distance decreases from 1.175(5) to 1.140(7) Å]. The bond lengths at rhodium are changed by amounts below the level of experimental uncertainties, with the exception of the precisely determined Rh–Cl distance which decreases slightly from 2.354(1) to 2.340(2) Å. These changes are all in line with the conclusion that oxidation is largely localised at manganese and has minor effects on the axial ligands at manganese. As a result there is limited transmission of such effects to rhodium, in full accord with the ESR and IR spectroscopic data.

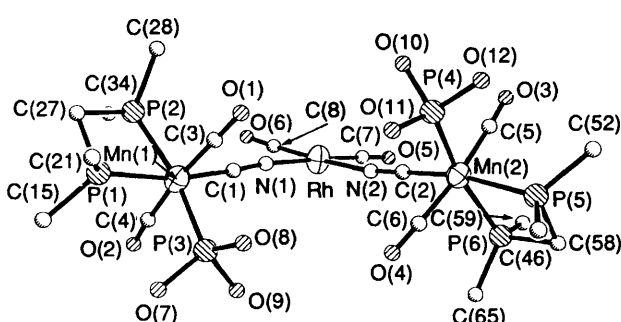
As noted above, the reaction of *trans*-[Mn(CN)(CO)(dppm)<sub>2</sub>][PF<sub>6</sub>]<sup>-</sup> with [{Rh(μ-Cl)(CO)<sub>2</sub>}]<sup>2+</sup> provides the best route to [*trans*-(dppm)<sub>2</sub>(OC)Mn(μ-CN)Rh(CO)<sub>2</sub>Cl][PF<sub>6</sub>]<sup>-</sup>. On mixing *trans*-[Mn(CN)(CO)<sub>2</sub>(PEt<sub>3</sub>)(dppe)]<sup>+</sup> with [{Rh(μ-Cl)(CO)<sub>2</sub>}]<sup>2+</sup> in CH<sub>2</sub>Cl<sub>2</sub>, the IR carbonyl spectrum showed bands at 2089, 2020 and 1980 cm<sup>-1</sup> consistent with the formation of [*trans*-(dppe)(Et<sub>3</sub>P)(OC)<sub>2</sub>Mn(μ-CN)Rh(CO)<sub>2</sub>Cl]<sup>+</sup>, i.e. of an analogue of [*trans*-(dppm)<sub>2</sub>(OC)Mn(μ-CN)Rh(CO)<sub>2</sub>Cl]<sup>+</sup>. However, within 30 min these bands were completely replaced by those of [*cis*-(dppe)(Et<sub>3</sub>P)(OC)<sub>2</sub>Mn(μ-CN)Rh(CO)<sub>2</sub>Cl]<sup>+</sup> and an unidentified complex containing no Rh(CO)<sub>2</sub> group. Similarly, the reaction of *trans*-[Mn(CN)(CO)<sub>2</sub>{P(OEt)<sub>3</sub>}<sub>2</sub>](dppm)<sup>+</sup> with [{Rh(μ-Cl)(CO)<sub>2</sub>}]<sup>2+</sup> in CH<sub>2</sub>Cl<sub>2</sub> led to the observation of bands at 2089, 2022 and 2002 cm<sup>-1</sup>, consistent with [*trans*-(dppm){(EtO)<sub>3</sub>P}(OC)<sub>2</sub>Mn(μ-CN)Rh(CO)<sub>2</sub>Cl]<sup>+</sup>. These bands were rapidly replaced by those of [*trans*-(dppm){(EtO)<sub>3</sub>P}(OC)<sub>2</sub>Mn(μ-CN)Rh(CO)<sub>2</sub>Cl]<sup>+</sup> before complete disruption of the Mn(CN)Rh skeleton. The manganese(II)-containing cations [*trans*-(dppe)(Et<sub>3</sub>P)(OC)<sub>2</sub>Mn(μ-CN)Rh(CO)<sub>2</sub>Cl]<sup>+</sup> and [*trans*-(dppm){(EtO)<sub>3</sub>P}(OC)<sub>2</sub>Mn(μ-CN)Rh(CO)<sub>2</sub>Cl]<sup>+</sup> are therefore unstable on the synthetic time-scale [cf. the results of cyclic voltammetry on [*trans*-(dppm){(RO)<sub>3</sub>P}(OC)<sub>2</sub>Mn(μ-CN)Rh(CO)<sub>2</sub>Cl] (R = Et or Ph) noted above].

**Heterotrinuclear Complexes.**—The complexes [*cis*-(dppm){(PhO)<sub>3</sub>P}(OC)<sub>2</sub>Mn(μ-CN)Rh(CO)<sub>2</sub>Cl]<sup>+</sup>, [*trans*-(dppm){(PhO)<sub>3</sub>P}(OC)<sub>2</sub>Mn(μ-CN)Rh(CO)<sub>2</sub>Cl]<sup>+</sup>, [*cis*-(dppe)(Et<sub>3</sub>P)(OC)<sub>2</sub>Mn(μ-CN)Rh(CO)<sub>2</sub>Cl]<sup>+</sup> and [*trans*-(dppm){(EtO)<sub>3</sub>P}(OC)<sub>2</sub>Mn(μ-CN)Rh(CO)<sub>2</sub>Cl]<sup>+</sup> undergo chloride abstraction with TIPF<sub>6</sub> in CH<sub>2</sub>Cl<sub>2</sub> to give, in the presence of the appropriate cyanomanganese ligand, good yields of the yellow or orange symmetrical heterotrinuclear complexes [*trans*-{(dppm)[(RO)<sub>3</sub>P](OC)<sub>2</sub>Mn(μ-CN)<sub>2</sub>Rh(CO)<sub>2</sub>][PF<sub>6</sub>]<sup>-</sup>] 7 (R = Et or Ph), [*cis*-{(dppm)[(PhO)<sub>3</sub>P](OC)<sub>2</sub>Mn(μ-CN)<sub>2</sub>Rh(CO)<sub>2</sub>][PF<sub>6</sub>]<sup>-</sup>] 8 and [*cis*-{(dppe)(Et<sub>3</sub>P)(OC)<sub>2</sub>Mn(μ-CN)<sub>2</sub>Rh(CO)<sub>2</sub>][PF<sub>6</sub>]<sup>-</sup>] (Table 1). Attempts to prepare asymmetric trinuclear species containing two different cyanomanganese ligands, for example from [*cis*-(dppm){(PhO)<sub>3</sub>P}(OC)<sub>2</sub>Mn(μ-CN)Rh(CO)<sub>2</sub>Cl] and *cis*-[Mn(CN)(CO)<sub>2</sub>(PEt<sub>3</sub>)(dppe)] in the presence of TIPF<sub>6</sub> also gave yellow [PF<sub>6</sub>]<sup>-</sup> salts. Although the elemental analyses (C, H and N) were correct for the expected products, all of the spectroscopic and electrochemical data obtained were also consistent with 1:1 mixtures of the two corresponding symmetrical heterotrinuclear complexes (i.e. the expected products of the disproportionation of the asymmetric species). Interestingly, the addition of *cis*-[Mn(CN)(CO)<sub>2</sub>(PEt<sub>3</sub>)(dppe)] to [*cis*-(dppm){(RO)<sub>3</sub>P}(OC)<sub>2</sub>Mn(μ-CN)Rh(CO)<sub>2</sub>Cl] (R = Et or Ph) in the absence of TIPF<sub>6</sub> rapidly gave *cis*-[Mn(CN)(CO)<sub>2</sub>(PR<sub>3</sub>)(dppm)]<sup>+</sup> (R = OEt or OPh) and [*cis*-(dppe)(Et<sub>3</sub>P)(OC)<sub>2</sub>Mn(μ-CN)Rh(CO)<sub>2</sub>Cl]<sup>+</sup> showing the ready exchange of cyanomanganese ligands, i.e. that the Rh–NC bonds are indeed labile.

The gross structure of the symmetrical heterotrinuclear complexes was deduced from the IR spectra (Table 1). The two carbonyl bands observed for the Rh(CO)<sub>2</sub> unit show that the *cis* geometry is retained on chloride substitution by the second manganese ligand, and the shift to higher energy of those bands relative to those of the heterobinuclear complexes is in accord with a positively charged rhodium atom. Such a charge distribution is also in agreement with the shift to lower energy in the

**Table 4** Selected bond lengths ( $\text{\AA}$ ) and angles ( $^\circ$ ) for **7** ( $\text{R} = \text{Et}$ ) $\cdot$  $2\text{C}_6\text{H}_{14}$ 

Rh–N(1)	2.032(12)	Rh–N(2)	2.024(11)	Rh–C(7)	1.846(15)
Rh–C(8)	1.824(18)	Mn(1)–P(1)	2.280(4)	Mn(1)–P(2)	2.294(5)
Mn(1)–P(3)	2.212(6)	Mn(1)–C(1)	1.921(14)	Mn(1)–C(3)	1.803(16)
Mn(1)–C(4)	1.824(17)	Mn(2)–P(4)	2.218(5)	Mn(2)–P(5)	2.287(4)
Mn(2)–P(6)	2.303(5)	Mn(2)–C(2)	1.941(14)	Mn(2)–C(5)	1.852(17)
Mn(2)–C(6)	1.840(16)	P(1)–C(15)	1.829(14)	P(1)–C(21)	1.822(14)
P(1)–C(27)	1.841(17)	P(2)–C(27)	1.833(14)	P(2)–C(28)	1.810(15)
P(2)–C(34)	1.812(15)	P(3)–O(7)	1.608(13)	P(3)–O(8)	1.604(11)
P(3)–O(9)	1.598(14)	P(4)–O(10)	1.592(12)	P(4)–O(11)	1.601(10)
P(4)–O(12)	1.596(11)	P(5)–C(46)	1.830(13)	P(5)–C(52)	1.823(13)
P(5)–C(58)	1.860(16)	P(6)–C(58)	1.815(14)	P(6)–C(59)	1.788(14)
P(6)–C(65)	1.776(16)	N(1)–C(1)	1.174(18)	N(2)–C(2)	1.148(17)
O(1)–C(3)	1.160(19)	O(2)–C(4)	1.138(21)	O(3)–C(5)	1.117(20)
O(4)–C(6)	1.115(19)	O(5)–C(7)	1.144(19)	O(6)–C(8)	1.125(23)
O(7)–C(9)	1.536(27)	O(8)–C(11)	1.521(25)	O(9)–C(13)	1.471(21)
O(10)–C(40)	1.486(18)	O(11)–C(42)	1.491(23)	O(12)–C(44)	1.512(24)
N(1)–Rh–N(2)	90.1(5)	N(1)–Rh–C(7)	179.1(7)	N(2)–Rh–C(7)	89.5(6)
N(1)–Rh–C(8)	89.4(6)	N(2)–Rh–C(8)	176.4(8)	C(7)–Rh–C(8)	91.0(7)
P(1)–Mn(1)–P(2)	72.8(2)	P(1)–Mn(1)–P(3)	95.3(2)	P(2)–Mn(1)–P(3)	167.8(2)
P(1)–Mn(1)–C(1)	167.0(5)	P(2)–Mn(1)–C(1)	94.3(5)	P(3)–Mn(1)–C(1)	97.7(5)
P(1)–Mn(1)–C(3)	93.2(5)	P(2)–Mn(1)–C(3)	92.2(6)	P(3)–Mn(1)–C(3)	90.8(6)
C(1)–Mn(1)–C(3)	85.6(6)	P(1)–Mn(1)–C(4)	92.4(5)	P(2)–Mn(1)–C(4)	92.4(6)
P(3)–Mn(1)–C(4)	85.6(6)	C(1)–Mn(1)–C(4)	89.6(7)	C(3)–Mn(1)–C(4)	173.6(7)
P(4)–Mn(2)–P(5)	95.3(2)	P(4)–Mn(2)–P(6)	167.9(2)	P(5)–Mn(2)–P(6)	72.8(1)
P(4)–Mn(2)–C(2)	97.8(5)	P(5)–Mn(2)–C(2)	166.9(5)	P(6)–Mn(2)–C(2)	94.1(5)
P(4)–Mn(2)–C(5)	86.3(5)	P(5)–Mn(2)–C(5)	94.6(4)	P(6)–Mn(2)–C(5)	91.9(5)
C(2)–Mn(2)–C(5)	87.5(6)	P(4)–Mn(2)–C(6)	91.8(5)	P(5)–Mn(2)–C(6)	92.6(5)
P(6)–Mn(2)–C(6)	91.4(6)	C(2)–Mn(2)–C(6)	85.7(6)	C(5)–Mn(2)–C(6)	172.6(6)
Mn(1)–P(1)–C(15)	122.0(5)	Mn(1)–P(1)–C(21)	123.5(4)	C(15)–P(1)–C(21)	102.4(6)
Mn(1)–P(1)–C(27)	96.1(4)	C(15)–P(1)–C(27)	105.7(6)	C(21)–P(1)–C(27)	104.2(7)
Mn(1)–P(2)–C(27)	95.8(5)	Mn(1)–P(2)–C(28)	123.1(5)	C(27)–P(2)–C(28)	104.7(7)
Mn(1)–P(2)–C(34)	121.7(6)	C(27)–P(2)–C(34)	108.0(6)	C(28)–P(2)–C(34)	101.5(7)
Mn(1)–P(3)–O(7)	114.9(5)	Mn(1)–P(3)–O(8)	113.6(5)	O(7)–P(3)–O(8)	102.9(6)
Mn(1)–P(3)–O(9)	121.0(5)	O(7)–P(3)–O(9)	97.6(7)	O(8)–P(3)–O(9)	104.2(6)
Mn(2)–P(4)–O(10)	120.7(4)	Mn(2)–P(4)–O(11)	113.4(5)	O(10)–P(4)–O(11)	104.0(6)
Mn(2)–P(4)–O(12)	115.3(4)	O(10)–P(4)–O(12)	98.5(6)	O(11)–P(4)–O(12)	102.4(5)
Mn(2)–P(5)–C(46)	122.7(4)	Mn(2)–P(5)–C(52)	121.8(5)	C(46)–P(5)–C(52)	102.3(6)
Mn(2)–P(5)–C(58)	95.3(4)	C(46)–P(5)–C(58)	107.2(7)	C(52)–P(5)–C(58)	105.2(6)
Mn(2)–P(6)–C(58)	96.1(5)	Mn(2)–P(6)–C(59)	121.3(6)	C(58)–P(6)–C(59)	107.1(6)
Mn(2)–P(6)–C(65)	122.8(5)	C(58)–P(6)–C(65)	106.5(7)	C(59)–P(6)–C(65)	101.3(7)
Rh–N(1)–C(1)	173.5(14)	Rh–N(2)–C(2)	170.8(14)	P(3)–O(7)–C(9)	125.7(12)
P(3)–O(8)–C(11)	122.1(11)	P(3)–O(9)–C(13)	123.5(12)	P(4)–O(10)–C(40)	123.6(11)
P(4)–O(11)–C(42)	120.6(10)	P(4)–O(12)–C(44)	128.2(11)	Mn(1)–C(1)–N(1)	177.4(16)
Mn(2)–C(2)–N(2)	177.7(14)	Mn(1)–C(3)–O(1)	177.4(13)	Mn(1)–C(4)–O(2)	176.3(12)
Mn(2)–C(5)–O(3)	177.5(13)	Mn(2)–C(6)–O(4)	176.7(13)	Rh–C(7)–O(5)	176.2(18)
Rh–C(8)–O(6)	177.2(19)	P(1)–C(27)–P(2)	95.2(7)	P(5)–C(58)–P(6)	95.7(7)

**Fig. 3** Molecular structure of the cation of **7** ( $\text{R} = \text{Et}$ ) showing the atom labelling scheme. All of the hydrogen atoms, the ethyl group atoms and all but the *ipso* carbons of the phenyl groups have been omitted for clarity

stretching frequency for the bridging cyanides (for which only one absorption is observed) and with the invariance of  $\nu(\text{CO})$  for the  $\text{Mn}(\text{CO})_2$  groups of corresponding neutral binuclear and cationic trinuclear species.

A more detailed description of the structure of the trinuclear cations was provided by an X-ray diffraction study on single crystals of  $\{[\text{trans-}(\text{dppm})[(\text{EtO})_3\text{P}](\text{OC})_2\text{Mn}(\mu\text{-CN})\}_2\text{Rh-}$

$(\text{CO})_2\}[\text{PF}_6]\cdot 2\text{C}_6\text{H}_{14}$ . The results of the crystal structure analysis are summarised in Table 4 and illustrated in Fig. 3. As for **3** and **3<sup>+</sup>** the local co-ordination geometries at rhodium and manganese are respectively square planar and octahedral; the assignment of *cis*-(CO)<sub>2</sub> geometry at Rh and *trans*-(CO)<sub>2</sub> at Mn on the basis of the IR spectra is confirmed. The cation as a whole has approximate  $C_2$  symmetry (see Fig. 3) with the crowded MnP<sub>3</sub> planes inclined relative to the rhodium co-ordination plane (dihedral angles 43.9 and 50.4°). Given the results of our extended Hückel molecular orbital (EHMO) calculations<sup>5</sup> on *trans*-[Mn(CN)(CO)<sub>2</sub>(PH<sub>3</sub>)<sub>3</sub>]<sup>+</sup>, which should be a reasonable model for *trans*-[Mn(CN)(CO)<sub>2</sub>{P(OEt)<sub>3</sub>}<sub>2</sub>(dppm)]<sup>+</sup> we can be confident that the highest occupied molecular orbital (HOMO) of the latter largely comprises a d<sub>π</sub> orbital [*e.g.* d<sub>xz</sub> if the CN is on *z*, P(OEt)<sub>3</sub> is on *x*, and a CO is on *y*] in the Mn(CN)P<sub>3</sub> plane, *i.e.* the plane not containing the strongest π-acceptor ligands (CO). This orbital, or one containing a major contribution from it, is likely to be the HOMO of species such as **7** ( $\text{R} = \text{Et}$ ). When oxidised the orientation of this orbital is such that it can in principle interact with the CN π system and hence with the rhodium and the other manganese attached to it (see below). This argument should generally apply to all complexes of *trans*-(NC)Mn(CO)<sub>2</sub>P<sub>3</sub> ligands. In contrast complexes of *trans*-(NC)Mn(CO)P<sub>4</sub> in which oxidation removes an electron from

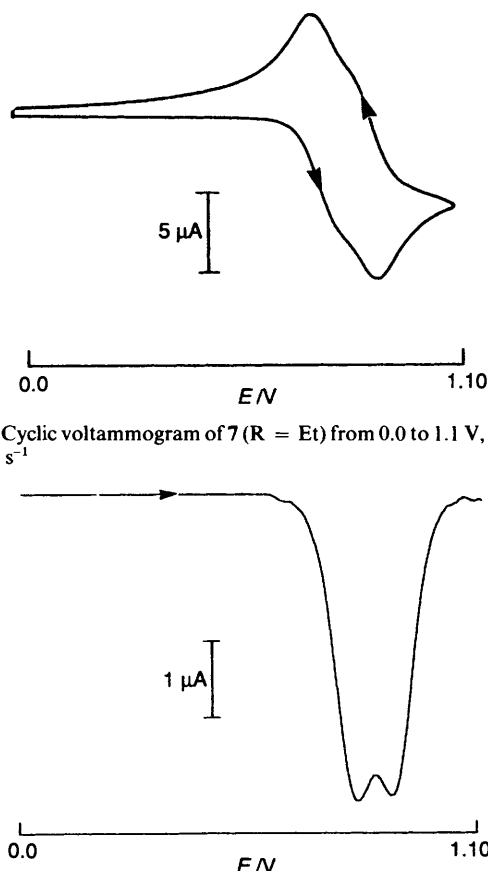


Fig. 4 Cyclic voltammogram of  $7$  ( $R = Et$ ) from 0.0 to 1.1 V, scan rate 100 mV s $^{-1}$

Fig. 5 Differential-pulse voltammogram of  $7$  ( $R = Et$ ) from 0.0 to 1.1 V, scan rate 2 mV s $^{-1}$

the equatorial Mn d<sub>z</sub><sup>2</sup> orbital in the MnP<sub>4</sub> plane, are likely to result in species for which 'communication' along the Mn-CN-M π system is less favoured because the singly occupied molecular orbital (SOMO) is of pseudo-δ symmetry with respect to the Mn-CN axis.

Electrochemical studies on heterotrinuclear complexes such as  $[\{trans\text{-}(dppm)\}[(EtO)_3P](OC)_2Mn(\mu\text{-CN})_2]_2Rh(CO)_2\text{-}[PF_6]$  have allowed us to probe the interaction of two redox-active cyanomanganese ligands through a symmetrical bridge, *i.e.* through the *cis*-Rh(CO)<sub>2</sub> group, and compare the interaction with that *via* the asymmetric cyanide bridge in homobinuclear complexes such as  $1^+$ . The voltammetry of complexes such as  $[\{cis\text{-}(dppm)\}[(EtO)_3P](OC)_2Mn(\mu\text{-CN})_2]_2Rh(CO)_2\text{-}[PF_6]$  is complicated because of the possibility of *cis-trans* isomerisation at both manganese centres on oxidation. However, the voltammetry of  $[\{trans\text{-}(dppm)\}[(RO)_3P](OC)_2\text{-}Mn(\mu\text{-CN})_2]_2Rh(CO)_2\text{-}[PF_6]$  ( $R = Et$  or Ph) is relatively straightforward and provides evidence for weak interaction between the two manganese-based redox centres.

The cyclic voltammogram of  $[\{trans\text{-}(dppm)\}[(EtO)_3P](OC)_2Mn(\mu\text{-CN})_2]_2Rh(CO)_2\text{-}[PF_6]$   $7$  ( $R = Et$ ) (Fig. 4) shows two closely spaced oxidation waves the potentials of which,  $E_1^\circ$  and  $E_2^\circ$ , were estimated to be 0.82 and 0.91 V respectively. [The cyclic voltammogram of the P(OPh)<sub>3</sub> analogue is very similar with  $E_1^\circ = 1.00$ ,  $E_2^\circ = 1.09$  V.] Better resolution of the two redox waves was obtained, however, by using both square-wave and differential-pulse voltammetry. The differential-pulse voltammogram of  $7$  ( $R = Et$ ) is shown in Fig. 5 ( $E_1^\circ = 0.80$ ,  $E_2^\circ = 0.88$  V) and the square-wave voltammogram was very similar ( $E_1^\circ = 0.82$ ,  $E_2^\circ = 0.90$  V).

The observation of two oxidation waves for  $[\{trans\text{-}(dppm)\}[(EtO)_3P](OC)_2Mn(\mu\text{-CN})_2]_2Rh(CO)_2\text{-}$  indicates the sequential formation, *on the voltammetric time-scale*, of  $[\{trans\text{-}(dppm)\}[(EtO)_3P](OC)_2Mn(\mu\text{-CN})_2]_2Rh(CO)_2\text{-}^{2+}$  and  $[\{trans\text{-}(dppm)\}[(EtO)_3P](OC)_2Mn(\mu\text{-CN})_2]_2Rh(CO)_2\text{-}^{3+}$ ; the separation,

ΔE, of the two waves by *ca.* 80–90 mV suggests the dication to be a weakly interacting, Class II, mixed-valence complex, *cf.* the separations of the two oxidation waves of  $[Fe_2(\mu\text{-L})_2]$  ( $\Delta E = 590$  mV),<sup>8</sup>  $[Fe_2(\mu\text{-L})(\eta\text{-C}_5H_5)_2]$  ( $\Delta E = ca.$  350 mV)<sup>9,10</sup> [ $L$  = fulvalene (bi-2,4-cyclopentadien-1-ylidene)],  $[Fe_2(\mu\text{-C}_5H_4CH_2C_5H_4)(\eta\text{-C}_5H_5)_2]$  ( $\Delta E = 100$  mV)<sup>11</sup> and  $[Fe_2(\mu\text{-C}_3H_4CH_2CH_2C_3H_4)(\eta\text{-C}_5H_5)_2]$  ( $\Delta E = 40$  mV)<sup>10</sup> and of  $[(NH_3)_5Ru(\mu\text{-L}')Ru(NH_3)_5]^{4+}$  ( $L' =$  pyrazine,  $\Delta E = 390$  mV;<sup>12</sup>  $L' = 4,4'$ -bipyridyl,  $\Delta E = ca.$  35–75 mV<sup>13</sup>) and  $[Cl(bipy)_2Ru(\mu\text{-L}')Ru(bipy)_2Cl]^{2+}$  ( $L' =$  pyrazine, bipy = 2,2'-bipyridyl)<sup>14</sup> where the mono-oxidised form of the first mentioned in each series is delocalised (Class III<sup>15</sup>) in character whereas the last mentioned is Class II.

Unfortunately, attempts to characterise the dications  $[\{trans\text{-}(dppm)\}(R_3P)(OC)_2Mn(\mu\text{-CN})_2]_2Rh(CO)_2\text{-}^{2+}$  further were unsuccessful. The addition of  $[N(C_6H_4Br-p)_3][SbCl_6]$  to  $[\{trans\text{-}(dppm)\}[(EtO)_3P](OC)_2Mn(\mu\text{-CN})_2]_2Rh(CO)_2\text{-}^+$  led only to decomposition, and electrolysis of the same complex in the cavity of an ESR spectrometer gave no evidence of the formation of identifiable paramagnetic products. Interestingly, the addition of a small amount (*ca.* 10 mol%) of *trans*-[Mn(CN)(CO)<sub>2</sub>{P(OEt)<sub>3</sub>}](dppm)<sup>+</sup> to  $[\{trans\text{-}(dppm)\}[(EtO)_3P](OC)_2Mn(\mu\text{-CN})_2]_2Rh(CO)_2\text{-}^+$  slowly gave (*ca.* 2 h)  $[\{cis\text{-}(dppm)\}[(EtO)_3P](OC)_2Mn(\mu\text{-CN})_2]_2Rh(CO)_2\text{-}^+$ , a reaction reminiscent of the isomerisation of *trans*-[MnBr(CO)<sub>2</sub>{P(OPh)<sub>3</sub>}(dppm)] to *cis*-[MnBr(CO)<sub>2</sub>{P(OPh)<sub>3</sub>}(dppm)] catalysed by *trans*-[MnBr(CO)<sub>2</sub>{P(OPh)<sub>3</sub>}(dppm)]<sup>+</sup>.<sup>16</sup>

## Conclusions

The complexes *trans*-[Mn(CN)(CO)(dppm)<sub>2</sub>]<sup>2+</sup> and *cis*- or *trans*-[Mn(CN)(CO)<sub>2</sub>{PR<sub>3</sub>}(L-L)] act as ligands to square-planar rhodium(I) centres. Infrared and ESR spectroscopy, and structural studies on the redox pair  $[\{trans\text{-}(dppm)\}_2(OC)Mn(\mu\text{-CN})Rh(CO)_2Cl]^Z$  ( $Z = 0$  or  $+1$ ), suggest that oxidation at the manganese(I) site of  $[L_xMn(\mu\text{-CN})Rh(CO)_2Cl]$  leads to a small increase in positive charge at rhodium but little delocalisation of unpaired electron density from the low-spin manganese(II) centre. By contrast, voltammetric studies of the heterotrinuclear complexes  $[\{trans\text{-}(dppm)\}[(RO)_3P](OC)_2Mn(\mu\text{-CN})_2]_2Rh(CO)_2\text{-}^+$  ( $R = Et$  or Ph) imply weak interaction between the two redox-active manganese centres through the *cis*-Rh(CO)<sub>2</sub> bridge of the mixed-valence dications. That communication between the redox-active cyanomanganese ligand and a second metal site (*via* the cyanide bridge) is favoured by *trans*-Mn(CN)(CO)<sub>2</sub>L<sub>3</sub> compared with *trans*-Mn(CN)(CO)L<sub>4</sub> provides support for the conclusions drawn from EHMO calculations<sup>5</sup> which suggest the cyanide group to be in the plane of the π-symmetry SOMO of the former (in the oxidised, Mn<sup>II</sup>, state) but orthogonal to that plane in the latter.

## Experimental

The preparation, purification and reactions of the complexes described were carried out under an atmosphere of dry nitrogen, using dried, distilled, deoxygenated solvents. Unless stated otherwise the complexes (*i*) were purified by dissolution in CH<sub>2</sub>Cl<sub>2</sub>, filtration, addition of hexane and reduction of the solvent volume *in vacuo* to induce precipitation, and (*ii*) are air-stable solids which dissolve in polar solvents such as CH<sub>2</sub>Cl<sub>2</sub> or tetrahydrofuran (THF) to give moderately air-sensitive solutions. All of the reactions were carried out in flasks shielded from light by aluminium foil; where necessary the progress of a reaction was monitored by IR spectroscopy. The compounds *cis*- and *trans*-[Mn(CN)(CO)<sub>2</sub>{P(OR)<sub>3</sub>}(dppm)] ( $R = Et$ <sup>1</sup> or Ph<sup>17</sup>), *cis*-[Mn(CN)(CO)<sub>2</sub>{PEt<sub>3</sub>}(dppe)],<sup>1</sup> *trans*-[Mn(CN)(CO)<sub>2</sub>{PR<sub>3</sub>}(L-L)} $[\text{PF}_6]$  ( $R = OEt$  or OPh, L-L = dppm; R = Et, L-L = dppe),<sup>18</sup> *trans*-[Mn(CO)(CN)(dppm)<sub>2</sub>] and *trans*-[Mn(CO)(CN)(dppm)<sub>2</sub>] $[\text{PF}_6]\text{-CH}_2\text{Cl}_2$ <sup>3</sup> were prepared by published methods. The salt TiPF<sub>6</sub> was purchased from Strem Chemicals.

Cyclic voltammetry was carried out as previously described,<sup>1</sup>

**Table 5** Structure analyses\*

Crystal data	<b>3</b>	<b>3</b> PF <sub>6</sub> ·1.5C <sub>6</sub> H <sub>14</sub>	<b>7</b> (R = Et)·2C <sub>6</sub> H <sub>14</sub>
Formula	C <sub>54</sub> H <sub>44</sub> ClMnNO <sub>3</sub> P <sub>4</sub> Rh	C <sub>63</sub> H <sub>65</sub> ClF <sub>6</sub> MnNO <sub>3</sub> P <sub>5</sub> Rh	C <sub>82</sub> H <sub>102</sub> F <sub>6</sub> Mn <sub>2</sub> N <sub>2</sub> O <sub>12</sub> P <sub>7</sub> Rh
<i>M</i>	1072.1	1346.3	1851.3
Space group (no.)	P2 <sub>1</sub> /n (no. 14)	P2 <sub>1</sub> /n (no. 14)	P2 <sub>1</sub> /c (no. 14)
<i>a</i> Å	12.884(3)	13.375(3)	11.986(3)
<i>b</i> Å	21.457(5)	13.077(3)	36.220(7)
<i>c</i> Å	18.908(5)	34.695(7)	21.692(5)
β/°	108.77(2)	95.28(2)	105.95(2)
<i>U</i> Å <sup>3</sup>	4949(2)	6042(2)	9054(3)
<i>D</i> <sub>c</sub> /g cm <sup>-3</sup>	1.44	1.48	1.36
<i>F</i> (000)	2184	2760	3832
μ(Mo-Kα)/cm <sup>-1</sup>	8.0	7.2	6.5
Data collection and reduction			
Crystal dimensions/mm	0.7 × 0.4 × 0.4	0.5 × 0.5 × 0.4	1.1 × 0.3 × 0.2
Colour	Orange	Red	Yellow
Crystallisation solvent	CH <sub>2</sub> Cl <sub>2</sub> -hexane	CH <sub>2</sub> Cl <sub>2</sub> -hexane	thf-hexane
2θ Range/°	4–50	4–47	4–50
Scan method	Wyckoff, ω	Wyckoff, ω	Wyckoff, ω
Scan width/ω/°	0.8	0.7	0.6
Total data	10 125	10 170	18 141
Unique data	8772	8923	15 945
'Observed' [F <sup>2</sup> > 2σ(F <sup>2</sup> )] data <i>N</i> <sub>o</sub>	6389	5838	6265
Minimum, maximum transmission coefficients	0.58, 0.73	0.41, 0.49	0.63, 0.69
Refinement			
Least-squares variables <i>N</i> <sub>v</sub>	586	743	750
<i>R</i>	0.042	0.049	0.089
<i>R'</i>	0.043	0.049	0.081
<i>S</i>	1.43	1.35	1.63
<i>g</i>	0.0005	0.0006	0.0008
Final difference map features/e Å <sup>-3</sup>	+0.73, -0.76	+0.38, -0.27	+0.74, -0.56

\* Details in common: crystal system, monoclinic; *Z* = 4; number of azimuthal scan data, 420; *R* = Σ|Δ|/Σ|F<sub>o</sub>|; *R'* = [ΣwΔ<sup>2</sup>/ΣwF<sub>o</sub><sup>2</sup>]<sup>1/2</sup>; *S* = [ΣwΔ<sup>2</sup>/(N<sub>o</sub> - N<sub>v</sub>)]<sup>1/2</sup>; Δ = F<sub>o</sub> - F<sub>c</sub>; *w* = [σ<sub>c</sub><sup>2</sup>(F<sub>o</sub>) + gF<sub>o</sub><sup>2</sup>]<sup>-1</sup>, σ<sub>c</sub><sup>2</sup>(F<sub>o</sub>) = variance in F<sub>o</sub> due to counting statistics.

**Table 6** Atomic coordinates (× 10<sup>4</sup>) for [*trans*-(dppm)<sub>2</sub>(OC)Mn(μ-CN)Rh(CO)<sub>2</sub>Cl] **3**

Atom	<i>x</i>	<i>y</i>	<i>z</i>	Atom	<i>x</i>	<i>y</i>	<i>z</i>
Rh	852(1)	561(1)	3286(1)	Mn	1517(1)	2798(1)	4353(1)
P(1)	1224(1)	3099(1)	3146(1)	P(2)	-334(1)	2935(1)	3807(1)
P(3)	1791(1)	2447(1)	5538(1)	P(4)	3349(1)	2633(1)	4883(1)
Cl(1)	-521(1)	914(1)	2207(1)	N(1)	1068(3)	1441(2)	3722(2)
O(1)	1950(3)	4096(2)	4881(2)	O(2)	2558(4)	40(2)	4611(3)
O(3)	517(5)	-712(2)	2631(3)	C(1)	1235(3)	1939(2)	3964(2)
C(2)	1768(4)	3579(2)	4675(2)	C(3)	1762(3)	2754(2)	2448(2)
C(4)	1477(4)	2151(2)	2193(3)	C(5)	1922(5)	1876(3)	1691(3)
C(6)	2647(5)	2203(3)	1433(4)	C(7)	2933(6)	2787(4)	1676(4)
C(8)	2497(5)	3071(3)	2181(3)	C(9)	1294(4)	3934(2)	2976(2)
C(10)	438(5)	4282(2)	2525(3)	C(11)	538(6)	4915(3)	2448(4)
C(12)	1507(6)	5210(3)	2797(4)	C(13)	2375(6)	4872(3)	3237(3)
C(14)	2275(5)	4240(2)	3336(3)	C(15)	-249(3)	2893(2)	2852(2)
C(16)	-1340(3)	2358(2)	3884(2)	C(17)	-1889(5)	2453(3)	4404(3)
C(18)	-2525(6)	1981(4)	4553(4)	C(19)	-2641(5)	1430(3)	4177(4)
C(20)	-2126(5)	1334(3)	3653(4)	C(21)	-1477(4)	1799(2)	3504(3)
C(22)	-1053(3)	3670(2)	3818(3)	C(23)	-1908(4)	3854(3)	3219(3)
C(24)	-2457(5)	4417(3)	3226(4)	C(25)	-2150(5)	4783(3)	3850(4)
C(26)	-1317(5)	4589(3)	4460(5)	C(27)	-761(5)	4041(3)	4441(4)
C(28)	1627(4)	1616(2)	5679(2)	C(29)	550(4)	1387(2)	5425(3)
C(30)	338(5)	772(3)	5550(3)	C(31)	1178(6)	378(3)	5925(3)
C(32)	2224(6)	599(3)	6153(3)	C(33)	2461(5)	1209(2)	6029(3)
C(34)	1292(4)	2790(2)	6262(2)	C(35)	1053(6)	2435(3)	6805(3)
C(36)	670(6)	2726(4)	7333(4)	C(37)	509(6)	3346(4)	7321(4)
C(38)	762(7)	3701(4)	6806(4)	C(39)	1161(6)	3427(3)	6283(3)
C(40)	3277(3)	2615(2)	5845(2)	C(41)	4049(3)	1908(2)	4809(3)
C(42)	3753(4)	1589(2)	4134(3)	C(43)	4262(5)	1033(3)	4067(4)
C(44)	5078(5)	801(3)	4673(4)	C(45)	5400(5)	1115(3)	5323(4)
C(46)	4909(4)	1675(3)	5400(3)	C(47)	4376(4)	3210(2)	4852(3)
C(48)	4953(5)	3146(3)	4354(4)	C(49)	5659(6)	3608(4)	4285(5)
C(50)	5825(6)	4131(3)	4731(5)	C(51)	5237(6)	4202(3)	5207(4)
C(52)	4531(4)	3751(2)	5286(3)	C(53)	1899(5)	254(3)	4107(3)
C(54)	634(6)	-224(3)	2875(4)				

**Table 7** Atomic coordinates ( $\times 10^4$ ) for  $[trans\text{-}(dppm)_2(\text{OC})\text{Mn}(\mu\text{-CN})\text{Rh}(\text{CO})_2\text{Cl}][\text{PF}_6] \cdot 1.5\text{C}_6\text{H}_{14}$  3 $^+$   $\text{PF}_6 \cdot 1.5\text{C}_6\text{H}_{14}$ 

Atom	<i>x</i>	<i>y</i>	<i>z</i>	Atom	<i>x</i>	<i>y</i>	<i>z</i>
Rh	3694(1)	2006(1)	281(1)	Mn	2422(1)	3240(1)	-1085(1)
P(1)	4099(1)	3476(1)	-1217(1)	P(3)	2096(1)	1537(1)	-1263(1)
P(2)	2914(1)	4907(1)	-887(1)	P(4)	786(1)	2853(1)	-932(1)
P(5)	1182(2)	808(2)	1447(1)	F(1)	810(5)	321(5)	1055(2)
F(2A)	1983(20)	150(26)	1621(6)	F(2B)	1115(22)	1898(9)	1338(7)
F(3A)	126(10)	740(19)	1579(6)	F(3B)	1927(12)	1357(20)	1205(5)
F(4A)	456(13)	1673(13)	1273(4)	F(4B)	1316(11)	-386(8)	1519(5)
F(5A)	2295(8)	750(11)	1375(6)	F(5B)	309(13)	318(12)	1636(4)
F(6)	1441(7)	1295(10)	1839(2)	Cl(1)	4968(1)	3238(1)	331(1)
O(1)	1520(4)	3968(4)	-1842(1)	O(2)	2174(4)	346(4)	200(2)
O(3)	4319(5)	1428(6)	1091(2)	N(1)	3276(4)	2494(4)	-269(1)
C(1)	2972(4)	2783(4)	-569(2)	C(2)	1878(5)	3692(5)	-1550(2)
C(3)	5112(4)	2591(5)	-1086(2)	C(4)	5476(6)	1979(5)	-1369(2)
C(5)	6241(6)	1309(6)	-1278(2)	C(6)	6658(6)	1225(6)	-910(3)
C(7)	6312(6)	1804(6)	-624(2)	C(8)	5530(5)	2489(5)	-710(2)
C(9)	4386(5)	3900(5)	-1692(2)	C(10)	3913(6)	3429(6)	-2016(2)
C(11)	4206(8)	3643(9)	-2375(2)	C(12)	4957(9)	4323(10)	-2413(3)
C(13)	5422(8)	4798(8)	-2100(3)	C(14)	5132(6)	4595(6)	-1735(2)
C(15)	4245(4)	4574(5)	-891(2)	C(16)	2684(5)	5997(5)	-1201(2)
C(17)	3425(6)	6717(5)	-1244(2)	C(18)	3216(7)	7583(6)	-1463(2)
C(19)	2281(7)	7752(6)	-1642(2)	C(20)	1548(6)	7043(6)	-1605(2)
C(21)	1746(5)	6164(5)	-1387(2)	C(22)	2692(4)	5365(4)	-410(2)
C(23)	1936(5)	6057(5)	-369(2)	C(24)	1722(5)	6341(6)	4(2)
C(25)	2249(6)	5938(6)	323(2)	C(26)	2991(5)	5264(5)	281(2)
C(27)	3223(5)	4966(5)	-81(2)	C(28)	2293(6)	1131(5)	-1750(2)
C(29)	1686(7)	1490(6)	-2067(2)	C(30)	1920(9)	1255(8)	-2439(2)
C(31)	2717(11)	687(9)	-2495(3)	C(32)	3277(10)	300(7)	-2195(3)
C(33)	3104(7)	537(6)	-1814(3)	C(34)	2508(5)	474(5)	-958(2)
C(35)	1876(6)	-339(5)	-916(2)	C(36)	2216(7)	-1176(6)	-691(2)
C(37)	3159(8)	-1192(7)	-514(3)	C(38)	3800(7)	-382(6)	-554(2)
C(39)	3476(5)	469(5)	-776(2)	C(40)	747(5)	1692(5)	-1230(2)
C(41)	-307(4)	3607(5)	-1104(2)	C(42)	-295(5)	4645(5)	-1027(2)
C(43)	-1095(6)	5247(6)	-1161(2)	C(44)	-1912(7)	4816(8)	-1358(2)
C(45)	-1957(6)	3785(8)	-1419(2)	C(46)	-1150(5)	3173(6)	-1291(2)
C(47)	579(5)	2511(5)	-446(2)	C(48)	20(6)	1651(5)	-355(2)
C(49)	-83(7)	1439(6)	38(3)	C(50)	321(7)	2065(8)	318(2)
C(51)	859(6)	2902(8)	234(2)	C(52)	981(5)	3131(6)	-147(2)
C(53)	2751(6)	1002(6)	231(2)	C(54)	4069(6)	1634(7)	784(2)
C(55)	1088(41)	5695(48)	2479(16)	C(56)	701(24)	6702(24)	2505(9)
C(57)	336(15)	6988(15)	2838(7)	C(58)	1768(47)	7305(48)	2568(21)
C(59)	1162(53)	7030(47)	2888(17)	C(60)	1213(33)	7922(32)	3288(14)
C(61)	1249(21)	7792(20)	2317(7)	C(62)	2200(31)	8064(32)	2330(11)
C(63)	3206(30)	7972(29)	2301(11)	C(64)	3188(45)	8472(47)	2664(17)
C(65)	3419(43)	9561(50)	2510(17)	C(66)	2704(26)	8786(27)	2337(9)
C(67)	4235(21)	8611(21)	2522(8)	C(68)	4399(19)	9402(22)	2777(7)

on analytically pure, crystalline samples. Square-wave and differential-pulse voltammetry were carried out using the PAR Model 270 Electrochemical Analysis Software. Under the conditions used,  $E^\circ$  for the couples  $[\text{Fe}(\eta\text{-C}_5\text{H}_5)_2]^+ - [\text{Fe}(\eta\text{-C}_5\text{H}_5)_2]$  and  $[\text{Fe}(\eta\text{-C}_5\text{Me}_5)_2]^+ - [\text{Fe}(\eta\text{-C}_5\text{Me}_5)_2]$ , used as internal standards, are 0.47 and -0.09 V respectively. Infrared spectra were recorded on a Nicolet 5ZDX FT spectrometer, and  $X$ -band ESR spectra on a Bruker 300ESP spectrometer and calibrated against a solid sample of the diphenylpicrylhydrazyl (dpph) radical. Magnetic susceptibilities were determined at room temperature using a Sherwood magnetic susceptibility balance. Microanalyses were carried out by the staff of the Microanalytical Service of the School of Chemistry, University of Bristol.

**cis-[1,2-Bis(diphenylphosphino)ethane-1κ<sup>2</sup>P,P']tetracarbonyl-1κ<sup>2</sup>C,2κ<sup>2</sup>C-chloro-2κCl-(μ-cyano-1κC:2κN)(triethylphosphine-1κP)manganeserhodium**, [cis-(dppe)(Et<sub>3</sub>P)(OC)<sub>2</sub>Mn(μ-CN)Rh(CO)<sub>2</sub>Cl].—To a stirred solution of *cis*-[Mn(CN)(CO)<sub>2</sub>(PEt<sub>3</sub>)(dppe)] (70 mg, 0.11 mmol) in CH<sub>2</sub>Cl<sub>2</sub> (20 cm<sup>3</sup>) was added [{Rh(μ-Cl)(CO)<sub>2</sub>}<sub>2</sub>] (21 mg, 0.05 mmol). After 2 min the yellow solution was filtered and hexane (30 cm<sup>3</sup>) was added to precipitate the product. Purification from CH<sub>2</sub>Cl<sub>2</sub>-

hexane, followed by washing the product with ethanol gave a yellow solid, yield 54 mg (60%).

The complexes  $[cis\text{-}(dppm)\{\text{RO}_3\text{P}\}(\text{OC})_2\text{Mn}(\mu\text{-CN})\text{Rh}(\text{CO})_2\text{Cl}]$  5 (R = Et or Ph) and  $[trans\text{-}(dppm)\{\text{RO}_3\text{P}\}(\text{OC})_2\text{Mn}(\mu\text{-CN})\text{Rh}(\text{CO})_2\text{Cl}]$  4 (R = Et or Ph) and  $[trans\text{-}(dppm)_2(\text{OC})\text{Mn}(\mu\text{-CN})\text{Rh}(\text{CO})_2\text{Cl}]$  3 were prepared similarly although in most cases it was not necessary to wash the purified product with ethanol. The complexes were crystallised by allowing a concentrated CH<sub>2</sub>Cl<sub>2</sub> solution to diffuse into hexane at -10 °C.

{trans-Bis[bis(diphenylphosphino)methane-1κ<sup>2</sup>P,P']}tricarbonyl-1κC,2κ<sup>2</sup>C-chloro-2κCl-(μ-cyano-1κC:2κN)manganese-rhodium Hexafluorophosphate, [trans-(dppm)<sub>2</sub>(OC)Mn(μ-CN)Rh(CO)<sub>2</sub>Cl][PF<sub>6</sub>].—To a stirred solution of [{Rh(μ-Cl)(CO)<sub>2</sub>}<sub>2</sub>] (36 mg, 0.093 mmol) in CH<sub>2</sub>Cl<sub>2</sub> (50 cm<sup>3</sup>) was added trans-[Mn(CN)(CO)(dppm)<sub>2</sub>][PF<sub>6</sub>]·CH<sub>2</sub>Cl<sub>2</sub> (204 g, 0.184 mmol). After 5 min the bright red solution was filtered through Celite, hexane was added, and the volume of the mixture was reduced *in vacuo* to induce precipitation. Purification from CH<sub>2</sub>Cl<sub>2</sub>-hexane gave red microcrystals which were further purified by allowing a concentrated CH<sub>2</sub>Cl<sub>2</sub> solution of the product to diffuse into hexane at -10 °C, yield 157 mg (70%).

**Table 8** Atomic coordinates ( $\times 10^4$ ) for 7 (R = Et) · 2C<sub>6</sub>H<sub>14</sub>

Atom	<i>x</i>	<i>y</i>	<i>z</i>	Atom	<i>x</i>	<i>y</i>	<i>z</i>
Rh	5 728(1)	320(1)	3 899(1)	Mn(1)	7 605(2)	1 394(1)	5 351(1)
Mn(2)	3 892(2)	1 224(1)	2 104(1)	P(1)	8 256(3)	1 815(1)	6 152(2)
P(2)	7 001(4)	1 199(1)	6 213(2)	P(3)	8 417(4)	1 665(1)	4 668(2)
P(4)	3 025(4)	1 564(1)	2 687(2)	P(5)	3 244(3)	1 567(1)	1 190(2)
P(6)	4 547(3)	940(1)	1 319(2)	P(7)	5 444(10)	1 403(2)	8 814(4)
F(1)	5 905(28)	1 678(6)	8 485(16)	F(2)	4 881(21)	1 097(6)	9 184(9)
F(3)	5 561(18)	1 093(4)	8 376(7)	F(4)	5 163(29)	1 676(6)	9 274(10)
F(5)	4 248(20)	1 467(7)	8 361(8)	F(6)	6 526(17)	1 300(6)	9 311(9)
N(1)	6 391(12)	752(3)	4 482(6)	N(2)	5 118(10)	672(3)	3 158(6)
O(1)	5 391(10)	1 788(3)	4 794(5)	O(2)	9 757(11)	949(3)	5 724(6)
O(3)	1 821(10)	738(3)	1 856(6)	O(4)	6 073(10)	1 646(3)	2 558(6)
O(5)	4 810(13)	-299(3)	3 014(6)	O(6)	6 462(18)	-175(4)	5 017(7)
O(7)	9 583(11)	1 892(3)	4 995(5)	O(8)	7 605(10)	1 969(3)	4 225(5)
O(9)	8 908(11)	1 428(3)	4 180(5)	O(10)	2 532(9)	1 379(3)	3 224(5)
O(11)	3 811(9)	1 897(3)	3 053(5)	O(12)	1 874(10)	1 771(3)	2 294(4)
C(1)	6 876(14)	994(4)	4 808(7)	C(2)	4 641(13)	874(4)	2 765(7)
C(3)	6 271(14)	1 642(4)	5 016(7)	C(4)	8 942(16)	1 126(4)	5 600(7)
C(5)	2 590(15)	925(4)	1 936(7)	C(6)	5 239(14)	1 494(4)	2 373(7)
C(7)	5 142(16)	-71(4)	3 362(8)	C(8)	6 197(19)	9(5)	4 582(9)
C(9)	10 826(19)	1 743(7)	5 132(12)	C(10)	11 456(30)	1 959(8)	4 832(16)
C(11)	8 013(18)	2 199(6)	3 741(9)	C(12)	7 171(23)	2 467(7)	3 507(13)
C(13)	8 186(18)	1 180(5)	3 695(9)	C(14)	8 731(20)	826(7)	3 748(13)
C(15)	9 794(12)	1 857(4)	6 580(6)	C(16)	10 386(13)	1 557(4)	6 896(6)
C(17)	11 563(14)	1 580(4)	7 221(7)	C(18)	12 131(15)	1 902(5)	7 200(8)
C(19)	11 553(15)	2 205(5)	6 884(8)	C(20)	10 390(14)	2 187(4)	6 562(7)
C(21)	7 763(12)	2 292(4)	6 103(7)	C(22)	7 330(13)	2 471(4)	5 528(8)
C(23)	6 941(15)	2 838(5)	5 508(9)	C(24)	7 009(15)	3 005(5)	6 075(9)
C(26)	7 785(13)	2 473(4)	6 679(8)	C(25)	7 393(16)	2 841(5)	6 639(10)
C(27)	7 568(13)	1 598(4)	6 722(7)	C(28)	5 488(12)	1 172(4)	6 202(6)
C(29)	4 648(13)	1 069(4)	5 656(7)	C(30)	3 484(15)	1 019(4)	5 663(8)
C(31)	3 181(16)	1 094(4)	6 216(8)	C(32)	3 987(15)	1 191(4)	6 763(8)
C(33)	5 117(14)	1 231(4)	6 754(7)	C(34)	7 580(14)	785(4)	6 654(8)
C(35)	7 842(15)	763(5)	7 309(9)	C(36)	8 262(17)	428(6)	7 629(10)
C(37)	8 327(17)	139(6)	7 273(10)	C(38)	8 054(18)	150(6)	6 634(11)
C(39)	7 702(15)	482(5)	6 309(9)	C(40)	3 262(15)	1 172(5)	3 782(7)
C(41)	2 630(24)	841(5)	3 815(11)	C(42)	3 344(16)	2 165(5)	3 440(9)
C(43)	4 198(19)	2 454(5)	3 590(10)	C(44)	629(17)	1 646(7)	2 178(10)
C(45)	86(25)	1 808(8)	2 584(14)	C(46)	3 762(11)	2 035(3)	1 112(6)
C(47)	3 791(13)	2 160(4)	509(7)	C(48)	4 177(14)	2 528(5)	478(9)
C(49)	4 454(14)	2 743(5)	986(8)	C(50)	4 500(14)	2 633(4)	1 607(7)
C(51)	4 120(12)	2 260(4)	1 638(7)	C(52)	1 706(12)	1 601(4)	768(6)
C(53)	1 083(14)	1 273(4)	531(7)	C(54)	-89(16)	1 304(5)	218(8)
C(55)	-622(16)	1 636(5)	162(8)	C(56)	-58(16)	1 948(5)	391(8)
C(57)	1 130(14)	1 935(4)	707(7)	C(58)	3 874(13)	1 261(4)	683(7)
C(59)	4 071(12)	487(4)	1 038(7)	C(60)	3 844(14)	384(5)	403(8)
C(61)	3 591(15)	13(5)	221(9)	C(62)	3 613(15)	-244(5)	678(8)
C(63)	3 795(14)	-156(5)	1 296(8)	C(64)	4 039(13)	212(4)	1 471(8)
C(65)	6 040(12)	920(4)	1 345(7)	C(66)	6 848(16)	855(4)	1 913(9)
C(67)	7 989(20)	826(5)	1 924(11)	C(68)	8 349(19)	847(5)	1 358(9)
C(69)	7 541(16)	902(4)	798(9)	C(70)	6 417(15)	951(4)	794(8)
C(71)	1 517(40)	1 627(14)	8 918(22)	C(72)	587(47)	1 410(13)	8 654(22)
C(73)	1 072(50)	1 809(16)	8 846(26)	C(74)	358(43)	2 135(12)	8 430(22)
C(75)	1 314(43)	2 077(14)	8 853(23)	C(76)	-461(44)	1 934(14)	8 205(24)
C(77)	-271(46)	1 519(14)	8 422(23)	C(78)	2 224(68)	546(21)	8 568(32)
C(79)	1 753(58)	704(17)	7 913(34)	C(80)	2 493(69)	561(19)	7 507(34)
C(81)	2 058(59)	192(17)	7 370(29)	C(82)	1 484(49)	541(16)	7 422(28)
C(83)	1 463(67)	381(25)	8 061(40)	C(84)	2 512(64)	200(18)	8 316(33)
C(85)	3 030(55)	529(18)	8 182(33)	C(86)	2 996(54)	214(18)	7 816(33)
C(87)	730(60)	188(19)	4 913(44)	C(88)	767(58)	74(17)	5 448(32)
C(89)	-356(79)	-16(23)	5 425(36)	C(90)	-328(52)	1 775(17)	8 471(28)
C(91)	319(67)	276(22)	62(41)	C(92)	105(39)	38(17)	589(21)
C(93)	54(48)	-296(17)	9 709(27)	C(94)	122(41)	-304(14)	373(24)

*Preparation of [{{trans-(dppm)}[(EtO)<sub>3</sub>P]}(OC)<sub>2</sub>Mn( $\mu$ -CN)}<sub>2</sub>Rh(CO)<sub>2</sub>][PF<sub>6</sub>].*—A mixture of *trans*-[Mn(CN)(CO)<sub>2</sub>·P(OEt)<sub>3</sub>](dppm)] (700 mg, 1.018 mmol), [{Rh( $\mu$ -Cl)(CO)<sub>2</sub>}<sub>2</sub>] (99 mg, 0.255 mmol) and TiPF<sub>6</sub> (196 mg, 0.560 mmol) in CH<sub>2</sub>Cl<sub>2</sub> (100 cm<sup>3</sup>) was stirred until the reaction was adjudged complete by IR spectroscopy (*ca.* 2 h). The yellow solution was filtered, hexane was added to the filtrate, and the mixture was reduced in volume *in vacuo* to induce precipitation. The product was isolated as yellow crystals by allowing a concentrated

solution in CH<sub>2</sub>Cl<sub>2</sub> to diffuse into hexane at -10 °C, yield 725 mg (85%).

The complexes [{*trans*-(dppm)}[(PhO)<sub>3</sub>P](OC)<sub>2</sub>Mn( $\mu$ -CN)<sub>2</sub>Rh(CO)<sub>2</sub>][PF<sub>6</sub>] and [{*cis*-(dppm)}[(PhO)<sub>3</sub>P](OC)<sub>2</sub>Mn( $\mu$ -CN)<sub>2</sub>Rh(CO)<sub>2</sub>][PF<sub>6</sub>] were prepared similarly (with reaction times of *ca.* 3 and 20 h respectively).

*X-Ray Crystal Structure Determinations of 3, 3<sup>+</sup> PF<sub>6</sub>·1.5-C<sub>6</sub>H<sub>14</sub> and 7 (R = Et) · 2C<sub>6</sub>H<sub>14</sub>.*—Many of the details of the

structure analyses are listed in Table 5. X-Ray diffraction measurements on single crystals mounted in thin-walled glass capillaries were made at ambient temperature ( $T = 293\text{ K}$ ) with graphite monochromated Mo-K $\alpha$  X-radiation ( $\lambda = 0.710\text{73}\text{ \AA}$ ) using Siemens four-circle P3m diffractometers. Cell dimensions for each analysis were determined from the setting angle values of 40, 15 and 42 centred reflections respectively in the range  $14 < 2\theta < 30^\circ$ .

For each structure analysis intensity data were collected for unique portions of reciprocal space and corrected for long-term intensity fluctuations, on the basis of the intensities of three check reflections repeatedly measured during data collection, and for Lorentz, polarisation and absorption effects, the last on the basis of azimuthal scan data. The structures were solved by heavy atom (Patterson and Fourier difference) methods, and refined by full-matrix least squares against  $F$ . For  $3^+\text{PF}_6\cdot1.5\text{C}_6\text{H}_{14}$  and  $7(\text{R} = \text{Et})\cdot2\text{C}_6\text{H}_{14}$  the solvent atomic positions were clearly subject to disorder. Various models were tested in which the solvent atom positions were subjected to weak restraints on interatomic distances to ensure realistic molecular geometries. Much better fits to the electron density and lower residuals were obtained by the final model in which the carbon atom sites were assigned at the positions of maximum electron density and refined without constraints although we note that the resultant geometry is not close to that expected for hexane. For all three structures, except as noted below, all non-hydrogen atoms were assigned anisotropic displacement parameters and refined without positional constraints. For  $3^+\text{PF}_6\cdot1.5\text{C}_6\text{H}_{14}$  solvent carbon atoms were assigned freely refined isotropic displacement parameters and refined with restraints on C...C distances; the  $[\text{PF}_6]^-$  ion was subject to 50:50 two-fold disorder [atoms F(2A-5A, 2B-5B)] and its geometry was restrained to be close to octahedral. For  $7(\text{R} = \text{Et})\cdot2\text{C}_6\text{H}_{14}$  solvent and phenyl carbon atoms were assigned freely refined isotropic displacement parameters. The solvent atoms and those of the phosphite ethyl groups were refined with restraints on interatomic distances. All hydrogen atoms [except those on the solvent molecules and the  $\text{P}(\text{OEt})_3$  groups] were included in the models refined and were constrained to ideal geometries (with  $\text{C}-\text{H} = 0.96\text{ \AA}$ ) with fixed isotropic displacement parameters.

Final difference syntheses showed no chemically significant features; the largest maxima were close to the metal, solvent or anion atoms. Refinements converged to residuals given in Table 5. Tables 6-8 report the positional parameters for the structure determinations. All calculations were made with programs of the SHELXTL-PLUS<sup>19</sup> system. Complex neutral-atom scattering factors were taken from ref. 20.

Additional material available from the Cambridge Crystallographic Data Centre comprises H-atom coordinates, thermal parameters and remaining bond lengths and angles.

### Acknowledgements

We thank the SERC for research studentships (to F. L. A., A. C. L. and G. M. R.), for post-doctoral assistance (G. H. W.) and for funds for the purchase of the ESR spectrometer, and Johnson Matthey plc for a generous loan of rhodium salts.

### References

- 1 G. A. Carriero, N. G. Connelly, M. C. Crespo, I. C. Quarmby, V. Riera and G. H. Worth, *J. Chem. Soc., Dalton Trans.*, 1991, 315.
- 2 G. A. Carriero, N. G. Connelly, S. Alvarez, E. Perez-Carreno and S. Garcia-Granda, *Inorg. Chem.*, 1993, **32**, 272.
- 3 A. Christofides, N. G. Connelly, H. J. Lawson, A. C. Loynes, A. G. Orpen, M. O. Simmonds and G. H. Worth, *J. Chem. Soc., Dalton Trans.*, 1991, 1595.
- 4 A. Christofides, N. G. Connelly, H. J. Lawson and A. C. Loynes, *J. Chem. Soc., Chem. Commun.*, 1990, 597.
- 5 G. A. Carriero, N. G. Connelly, E. Perez-Carreno, A. G. Orpen, A. L. Rieger, P. H. Rieger, V. Riera and G. M. Rosair, *J. Chem. Soc., Dalton Trans.*, submitted.
- 6 N. G. Connelly, M. J. Freeman, A. G. Orpen, A. R. Sheehan, J. B. Sheridan and D. A. Sweigart, *J. Chem. Soc., Dalton Trans.*, 1985, 1019; A. G. Orpen, N. G. Connelly, M. W. Whiteley and P. Woodward, *J. Chem. Soc., Dalton Trans.*, 1989, 1751.
- 7 A. G. Orpen and N. G. Connelly, *J. Chem. Soc., Chem. Commun.*, 1985, 1310; *Organometallics*, 1990, **9**, 1206.
- 8 W. H. Morrison, jun., S. Krogsrud and D. N. Hendrickson, *Inorg. Chem.*, 1973, **12**, 1998.
- 9 T. Matsumoto, M. Sato and A. Ichimura, *Bull. Chem. Soc. Jpn.*, 1971, **44**, 1720.
- 10 G. M. Brown, T. J. Meyer, D. O. Cowan, C. LeVanda, F. Kaufman, P. V. Roling and M. D. Rausch, *Inorg. Chem.*, 1975, **14**, 506.
- 11 J. E. Gorton, H. L. Lentzner and W. E. Watts, *Tetrahedron*, 1971, **27**, 4353.
- 12 C. Creutz and H. Taube, *J. Am. Chem. Soc.*, 1973, **95**, 1086.
- 13 G. M. Tom, C. Creutz and H. Taube, *J. Am. Chem. Soc.*, 1974, **96**, 7827.
- 14 R. W. Callahan, F. R. Keene, T. J. Meyer and D. J. Salmon, *J. Am. Chem. Soc.*, 1977, **99**, 1064.
- 15 M. B. Robin and P. Day, *Adv. Inorg. Chem. Radiochem.*, 1967, **10**, 247.
- 16 N. G. Connelly, S. J. Raven, G. A. Carriero and V. Riera, *J. Chem. Soc., Chem. Commun.*, 1986, 992.
- 17 G. A. Carriero, M. C. Crespo, V. Riera, M. G. Sanchez, M. L. Valin, D. Moreiras and X. Solans, *J. Organomet. Chem.*, 1986, **302**, 47; see also ref. 14 in G. Barrado, G. A. Carriero, C. Diaz-Valenzuela and V. Riera, *Inorg. Chem.*, 1991, **30**, 4416.
- 18 N. G. Connelly, K. A. Hassard, B. J. Dunne, A. G. Orpen, S. J. Raven, G. A. Carriero and V. Riera, *J. Chem. Soc., Dalton Trans.*, 1988, 1623.
- 19 G. M. Sheldrick, SHELXTL-PLUS, Revision 4.1, Göttingen, 1990.
- 20 *International Tables for X-Ray Crystallography*, Kynoch Press, Birmingham, 1974, vol. 4.

Received 30th November 1992; Paper 2/06384K